https://doi.org/10.22226/2410-3535-2022-3-197-202

Alumina-based ceramics reinforced with calcium hexaaluminate

N. Yu. Cherkasova†, R. I. Kuzmin, A. V. Felofyanova, K. A. Antropova,

R. R. Khabirov, N. Yu. Burkhinova

†cherkasova.2013@corp.nstu.ru

Novosibirsk State Technical University, Novosibirsk, 630073, Russia

In this study, alumina ceramics containing calcium hexaaluminate are investigated. The specimens are obtained by axial pressing of granulated powders and pressureless sintering. Fracture toughness is tested using the indentation method. Microhardness is determined by the Vickers method. XRD and microstructural studies using a scanning electron microscope are carried out. It was found that the use of $Ca(OH)_2$ leads to the formation of $CaAl_{12}O_{19}$ in sintered alumina ceramics. As the platelet content increases, the average length of the platelets increases from 2 to 3 μm. The width of the platelets is about 0.4 μm. Increasing the $CaAl_{12}O_{19}$ content decreases the size of Al_2O_3 grains. The average grain size of the alumina ceramics is 1.65 ± 0.02 μm. For the material containing 6 wt.% $CaAl_{12}O_{19}$ the average grain size is 0.95 ± 0.05 μm. An increase in the critical stress intensity factor for the formation of 6 wt.% $CaAl_{12}O_{19}$ in a material compared to alumina ceramics without additives has been established. The relative density of such a material is 95.3 ± 0.5%, microhardness is 1800 ± 50 HV, fracture toughness is 5.2 ± 0.4 MPa·m$^{1/2}$. The increase in fracture toughness of composites containing $CaAl_{12}O_{19}$ platelets is due to the fracture of platelets, crack bridging and crack deflection.

Keywords: $CaAl_{12}O_{19}$, alumina, fracture toughness, crack deflection, crack bridging.

1. Introduction

At present there is a research development aimed at the production of composite ceramics reinforced with hexaaluminates of different chemical compositions. Complex oxides of the composition $MeAl_{11}O_{18}$ and $MeAl_{12}O_{19}$ (where Me = Ca, Sr, Ce, Na, Ba, La) have a platelet structure and relatively weak interphase boundaries with matrix grains [1]. The formation of weak interfaces between platelets and matrix grains promotes crack branching and additional energy dissipation in the material volume. A deflection of the crack propagation trajectory and its closure due to the convergence of the opposite sides of the crack can also be observed [2].

The crystalline structure of hexaaluminates largely determines the morphology and grain shape of these compounds. Machida was one of the first to study their structure. In [3,4] Machida studied the flat crystals of hexaaluminates. The particles were 100 – 200 nm long and 10 – 20 nm wide, which indicates a strong suppression of crystal growth in the [001] direction. This is because the most preferred route for oxygen diffusion is through the mirror planes of symmetry in which the Me cations are located.

Compared to fibres and whiskers, *in situ* formed hexaaluminate platelets are characterized by a simpler manufacturing process, lower costs and the formation of a denser and more homogeneous microstructure [5]. Hexaaluminates may have a β-Al_2O_3 or magnetoplumbite structure. β-Al_2O_3 includes $SrAl_{12}O_{19}$ [6 – 8], $LaAl_{11}O_{18}$ [9,10] and Ba-β-Al_2O_3 [11,12]. The structure of magnetoplumbite typically consists of $CaAl_{12}O_{19}$ [13,14] and $LaMgAl_{11}O_{19}$ [15,16].

Researchers in the field of materials science and fracture mechanics have widely studied the effect of hexaaluminate platelets of different chemical compositions on the properties of alumina-based ceramic materials. Liu et al evaluated the efficiency of *in situ* formation of Ba-β-Al_2O_3 in alumina zirconia ceramics [5]. The authors found that the formation of Ba-β-Al_2O_3 in the sintered material led to increased fracture toughness due to the crack deflection and crack bridging effects. Simultaneously, increasing the Ba-β-Al_2O_3 content reduces the relative density and hardness of the material and increases fracture toughness. The authors also noted the positive effect of barium hexaaluminate on the residual strength of composites after heat shock tests, which they attribute to the hexagonal structure of Ba-β-Al_2O_3, capable of dissipating energy during crack propagation under thermal shock. The change in the crack propagation trajectories and the resulting increase in the level of the critical stress intensity factor during the introduction of barium hexaaluminate into the zirconia matrix is given in [12]. The authors also observed a reduction of the grain size of the matrix component due to the formation of hexaaluminate platelets. Sktani et al. [17] also show the effectiveness of introducing lanthana into the alumina zirconia matrix to improve the fracture toughness of ceramic materials. The formation of $LaAl_{11}O_{18}$ platelets made it possible to obtain a material with a fracture toughness of 8.8 MPa·m$^{1/2}$ at a hardness of 1792 HV and a porosity of 0.46%. Naga et al. [10] showed a similar effect of increasing fracture toughness with increasing lanthanum

hexaluminate content and attributed it to a change in the crack propagation path. Podzorova et al. [18] evaluated the effect of cerium-calcium hexaaluminate on the characteristics of alumina-zirconia ceramics. The results also established the effectiveness of using this additive to improve the fracture toughness of the composite.

$CaAl_{12}O_{19}$ has been investigated in many works aimed to analyze the efficiency of hexaaluminates in alumina ceramics [18–20]. Asmi et al. [21] found that the highest fracture toughness of alumina ceramics was observed in a material containing 5 wt.% $CaAl_{12}O_{19}$. When the platelet content is 15 wt.% and higher, the critical stress intensity factor decreases. Sktani et al. in [22] studied ZTA ceramics with CaO and $CaCO_3$ additives. The $CaAl_{12}O_{19}$ content in the sintered material did not exceed 6 wt.%. The maximum recorded fracture toughness value was about 6.5 $MPa \cdot m^{1/2}$.

The literature analysis has shown the efficiency of hexaaluminates of different chemical compositions for increasing the fracture toughness of oxide ceramic materials. Simultaneously, the platelet structure of these compounds led to the formation of additional porosity in the material and a decrease in density. Note that an increase in the fracture toughness of alumina ceramics is of great importance, as Al_2O_3-ceramic has a low critical stress intensity factor, not exceeding 3.5 $MPa \cdot m^{1/2}$ [23, 24]. Therefore, studies aimed at investigating the efficiency of $CaAl_{12}O_{19}$ formation in sintered alumina ceramics up to 6 wt.% are relevant. A special interest is a detailed study of the structure of the obtained composites. This will expand knowledge about the formation of $CaAl_{12}O_{19}$ platelet in the alumina matrix structure.

2. Materials and investigation methods

Powders of Al_2O_3 from Almatis CT3000 SG with a purity of 99.7% and $Ca(OH)_2$ were used as the starting material. $Ca(OH)_2$ was synthesized by precipitation from $Ca(NO_3)_2 \cdot 4H_2O$. Experimental specimens were prepared using the axial pressing technology of pre-granulated ceramic powder. This technology includes the following stages: dispersion of water suspensions, granulation, pressing, pressureless sintering of compacts.

The suspensions contained 60% solids, 40% distilled water. The deflocculant Dolapix CE 64 was used in the amount of 1% of the dry powder weight. The suspensions were dispersed and mixed in a ball mill for 24 hours. The diameter of the alumina milling balls was 10 mm. The rotation speed was 80 rpm. A 10% water solution of polyvinyl alcohol in the amount of 1% by weight of ceramic powder was used as a binder. The resulting suspensions were sprayed through a two-fluid nozzle into liquid nitrogen. Then, sublimation drying of the obtained granules was carried out on a Scientz 10 ND unit.

The compacts were formed using the axial pressing technology at a pressure of 100 MPa on an Instron 3369 testing machine. Free sintering was carried out in a furnace (LHT 02/17, Naberterm) in air at 1520°C for 5 hours. The heating rate in the range of 25 – 900°C was 2°C/min. Heating rates above 900°C and cooling rates to room temperature were performed at 5°C/min. The dimensions of the sintered specimens in the shape of a bar were 4.5 × 4.5 × 45 mm.

The density of the sintered specimens was measured using the Archimedes method. The fracture toughness was determined by indentation with a load of 5 kg. The critical stress intensity factor was calculated using the formula given in [25]:

$$(K_{Ic}\phi/Ha^{1/2})(H/E\phi)^{2/5} = 0.035(l/a)^{-1/2}, \quad (1)$$

where K_{Ic} is the critical stress intensity factor, H is the Vickers hardness, E is Young's modulus, l is the crack length, a is the half-diagonal length of an indentation and ϕ is the constraint factor (≈3).

Vickers microhardness was measured using a 402MVD microhardness tester (Wolpert Group, Bretzfeld, Germany). The load on the diamond indenter was 500 g. X-ray phase analysis was performed on a Thermoscientific ARL X'TRA θ-2θ diffractometer using the ICDD PDF 4+ 2021 database. The diffraction patterns were obtained in copper K_α radiation. For microstructural studies specimens were cut and polished to a size of 1 μm and thermally etched at 1420°C for 1 hour. Microstructural studies were conducted using a Carl Zeiss Sigma microscope in the secondary electron emission mode.

3. Results and discussion

Figure 1 presents XRD patterns of the analysed materials. α-Al_2O_3 was detected. The $CaAl_{12}O_{19}$ reflexes are fixed in materials obtained using calcium hydroxide. The presence of other calcium aluminates was not detected.

Experimental specimens were obtained with a content of calcium hexaaluminate ranging from 0 to 6 wt.%. Table 1 shows the density and linear shrinkage values of the sintered materials. It has been found that the presence of calcium hexaaluminate leads to an insignificant decrease in the density of the material and an increase in linear shrinkage. The data are in agreement with various papers [5, 26]. The decrease in density is because Ca^{2+} inhibits the overall compaction rate due to the segregation of impurities at the Al_2O_3-grain boundaries [27]. Another reason is the elongated morphology of the hexaaluminate platelets, which limits the composite compaction. Simultaneously, the relative density of the composites obtained is at least 95% of the theoretical one. The appropriate amount of $CaAl_{12}O_{19}$ is favorable for the formation of dense Al_2O_3-ceramics.

Figure 2 presents the microstructure of ceramic materials. In all investigated materials the presence of equiaxed coarse grains representing alumina was detected. Platelet grains were fixed in the composite materials. EDX analysis determined that the platelets are composed of Ca and Al (Fig. 2e). Therefore, the results of EDX and XRD analyses prove that the platelets are calcium hexaaluminate. The platelets are predominantly evenly distributed. However, there are some $CaAl_{12}O_{19}$ agglomerates near which pore defects are recorded

Table 1. Density and shrinkage of the investigated materials.

$CaAl_{12}O_{19}$ content, wt.%	Apparent density, g/sm^3	Relative density, % of theoretical density	Linear shrinkage, %
0	3.90 ± 0.20	97.7 ± 0.3	17.9 ± 0.1
3	3.85 ± 0.25	96.7 ± 0.3	18.4 ± 0.2
6	3.79 ± 0.25	95.3 ± 0.5	18.9 ± 0.2

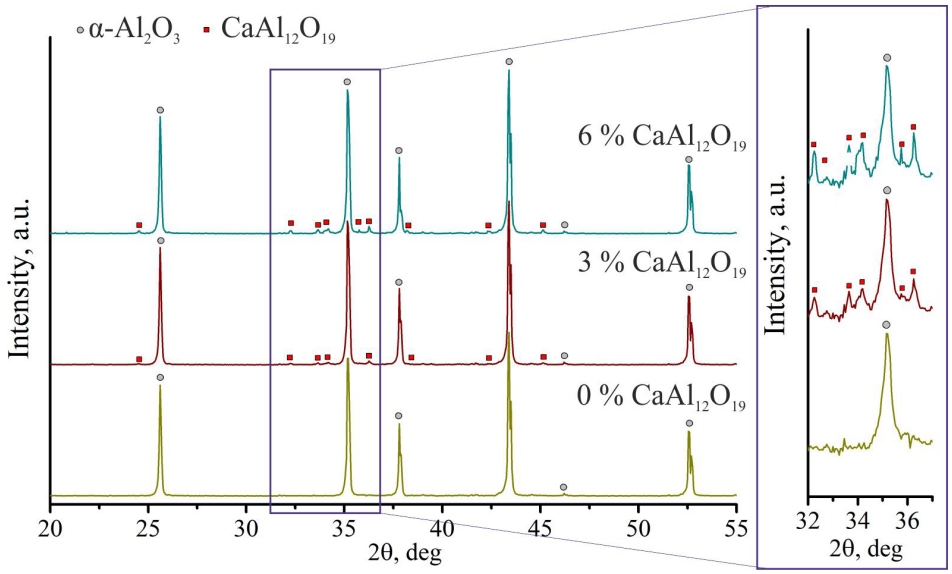

Fig. 1. (Color online) X-ray diffraction pattern of alumina ceramics containing calcium hexaaluminate.

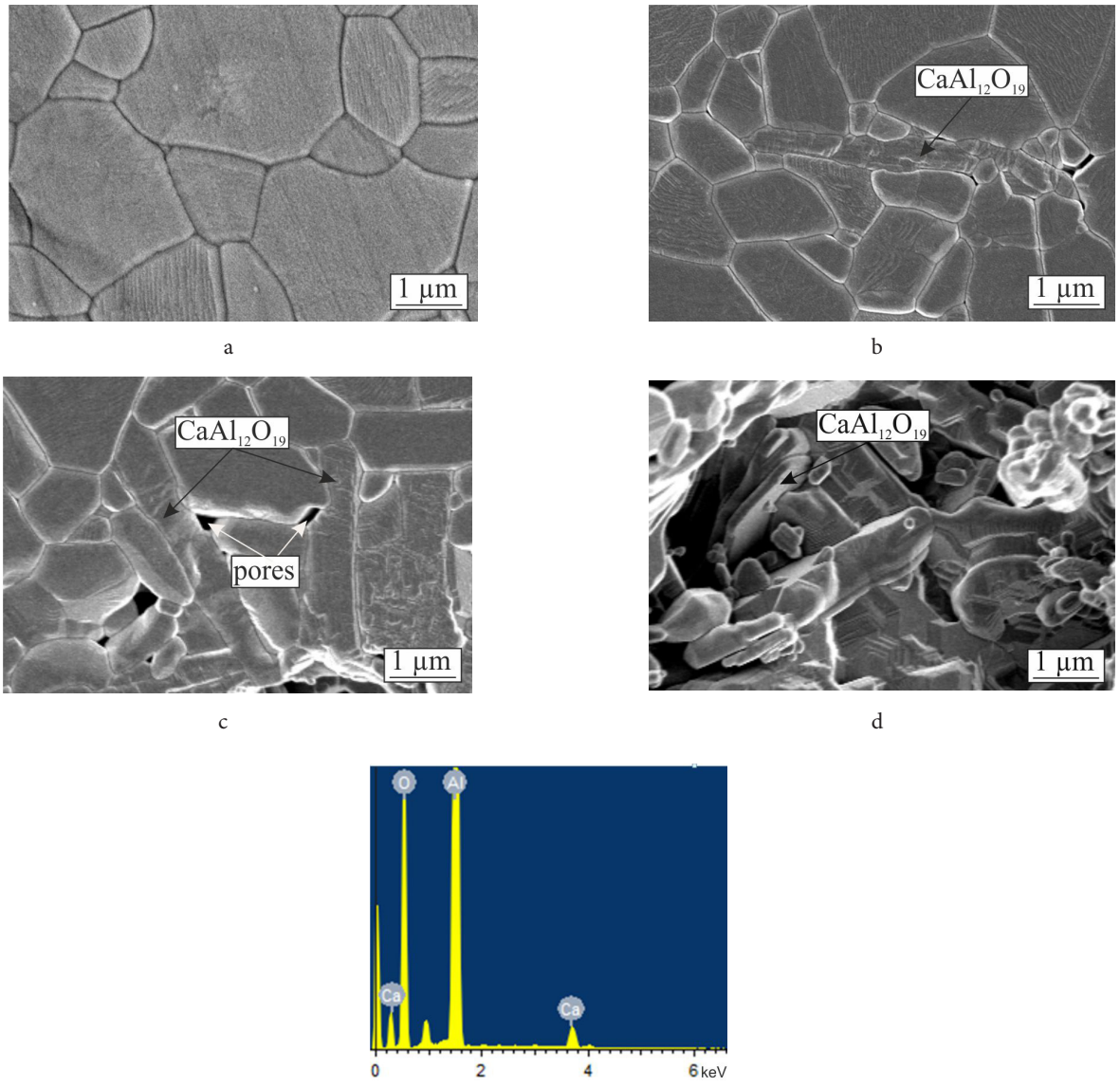

Fig. 2. Microstructure of sintered materials: alumina ceramics without additives (a); material with 3 wt.% $CaAl_{12}O_{19}$ (b); material with 6 wt.% $CaAl_{12}O_{19}$ (c); region with increased porosity and $CaAl_{12}O_{19}$ platelets (d); EDS pattern of the $CaAl_{12}O_{19}$ platelet (e).

(Fig. 2 c). Probably, the presence of pores is associated with the processes of $CaAl_{12}O_{19}$ synthesis occurring during sintering. An increase in the porosity of the materials correlates with a decrease in their relative density. Also, in the material with 6 wt.% $CaAl_{12}O_{19}$, the presence of a single region with high porosity in which the growth of $CaAl_{12}O_{19}$ platelets was not limited by Al_2O_3 grains was recorded (Fig. 2 d).

Analysis of the platelet structure showed that with 3 wt.% $CaAl_{12}O_{19}$ in the material the platelet length is about 2 μm, width is 0.4 μm. The aspect ratio is 5:1. In the material with 6 wt.% $CaAl_{12}O_{19}$, the platelet length averages 4 μm, with individual platelets up to 8–10 μm in length are present. The width of the platelets does not change significantly with their content in the composite. A fragmentary structure of the $CaAl_{12}O_{19}$ platelets was observed. Crystals mostly consist of a single platelet surrounded by equiaxed grains of alumina. Less frequently, platelets in the form of two or more platelets of the same size are found fused. Each platelet consists of a set of flat fragments, parallel to each other. The presence of boundaries between the fragments revealed by crystal chipping and thermal etching indicates their defective state. It can be explained by the action of residual stresses arising in the process of calcium hexaaluminate growth. A similar structure has been recorded for $SrAl_{12}O_{19}$ platelets in [28].

The microstructure analysis revealed a reduction of the size of alumina grains (Table 2). The percentages of grain size is reduced by 42% at 6 wt.% $CaAl_{12}O_{19}$. A similar effect was observed in materials containing hexaaluminates of different chemical composition [17, 26]. A decrease in the size of alumina grains with an increase in the content of $CaAl_{12}O_{19}$ is probably due to the effect of resistance of dissolved substances by segregated calcium ions on the mobility of Al_2O_3-grain boundaries [29]. Similar effects were also recorded by Amutha Rani et al. in [26] when studying the effect of rare-earth dopants on the properties of alumina ceramics. It was found that the reduction of alumina grain size with an increase in the content of lanthanum hexaaluminate increased the strength and fracture resistance of the materials. Sktani et al. [17] showed that the greater the La_2O_3 doping, the finer the Al_2O_3 grains, the stronger the interaction between the Al_2O_3 and $LaAl_{11}O_{18}$ grains.

The results of mechanical tests are shown in Table 3. The microhardness of the tested materials is somewhat reduced. This is due to a decrease in the content of alumina, which is consumed for the formation of $CaAl_{12}O_{19}$ in the composites, as well as an increase in the porosity in the materials. The critical stress intensity factor increases with increasing content of $CaAl_{12}O_{19}$ in the composites. In the material with 6 wt.% $CaAl_{12}O_{19}$, the fracture toughness was increased by 48% compared to alumina ceramics.

Figure 3 shows the crack propagation trajectories, characterizing the toughening mechanisms of alumina ceramics with calcium hexaaluminate. Alumina ceramics without additives are characterized by transcrystalline and intercrystalline fracture of grains. These mechanisms for increasing the fracture toughness are characteristic of both platelet-containing composites: platelets fracture, crack bridging, crack deflection. An example of the platelet fracture

Table 2. Alumina grain size of the investigated materials.

$CaAl_{12}O_{19}$ content, wt.%	Al_2O_3 average grain size, μm	Percentages of grain size decreases, %
0	1.65 ± 0.02	0
3	1.06 ± 0.03	36
6	0.95 ± 0.05	42

Table 3. Microhardness and fracture toughness of the investigated materials.

$CaAl_{12}O_{19}$ content, wt.%	Microhardness, HV	Fracture toughness, $MPa \cdot m^{1/2}$
0	1950 ± 100	3.5 ± 0.5
3	1850 ± 50	4.5 ± 0.4
6	1800 ± 50	5.2 ± 0.4

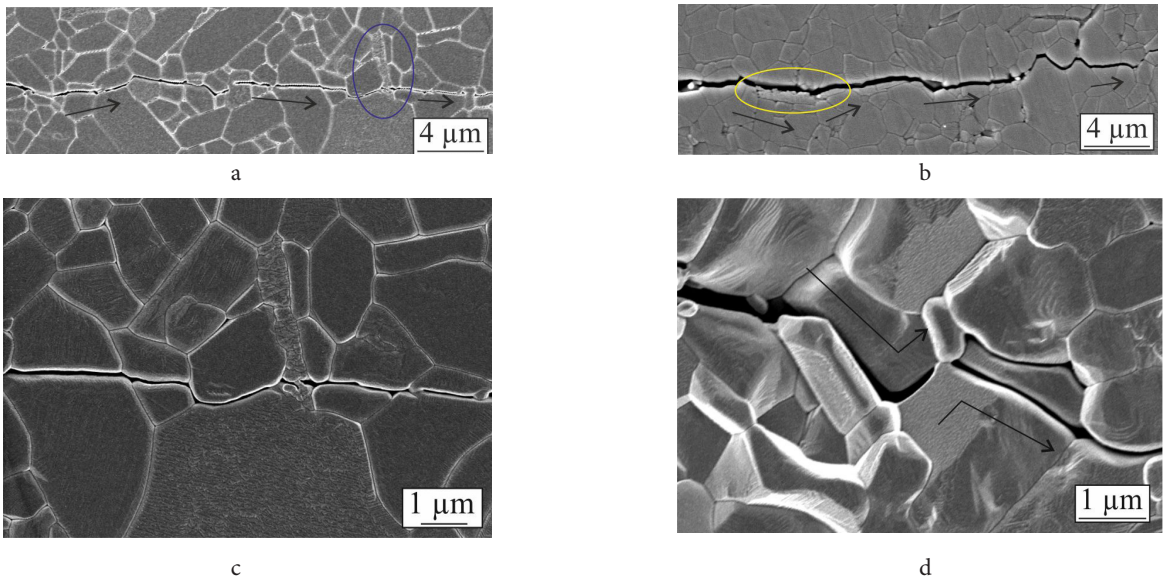

a b c d

Fig. 3. Microphotographs of crack propagation path for different materials: Al_2O_3 ceramics with 3 wt.% $CaAl_{12}O_{19}$ (platelets fracture) (a, c); Al_2O_3 ceramics with 6 wt.% $CaAl_{12}O_{19}$ (crack deflection) (b, d).

is shown in Fig. 3 c. This effect is explained by the platelet structure of calcium hexaaluminate and the lower strength between the layers compared to the cohesive strength between the platelet and the Al_2O_3 matrix. The structure of calcium hexaaluminate consists of spinel blocks formed by $A1^{3+}$ and O^{2-}. Between the blocks are large cations Ca^{2+} [28, 30]. The small number of inter-atomic bonds and the large distances between spinel blocks explains the low cohesive strength of the analyzed phase [31]. Zhang et al. [32] also reported $CaAl_{12}O_{19}$ platelet fractures and bridge formation. Shi et al. [33] investigated alumina ceramics with $SmAlO_3$ platelets and similar toughening mechanisms were observed. The crack deflection effect was detected in a material with 6 wt.% $CaAl_{12}O_{19}$ (Fig. 3 d). On impact with the platelet, the crack propagates along its interfaces and changes its propagation trajectory. Crack deflection is explained to the change of stress distribution in composites caused by $CaAl_{12}O_{19}$ [34]. The crack narrows and stops as a result. In materials with a small amount of calcium hexaaluminate the distance between the platelets is large. The platelets located far from each other cannot deflect the crack propagation trajectory.

Crack bridging was recorded in the material with 6 wt.% $CaAl_{12}O_{19}$. In this material, the platelet length is twice as greater than in the material with 3 wt.% $CaAl_{12}O_{19}$. Furthermore, platelets up to 8 μm in length are observed. Such platelets have larger grain boundaries and stronger bonding force with Al_2O_3, the probability of platelet fracture is lower. As a result, the crack bridging mechanism dominates and is more effective at increasing the fracture toughness of the material. Similar effects were obtained by Shi et al. [35] in a study of Al_2O_3/Ti composites with $CeAl_{11}O_{18}$ platelets. The authors fixed the mechanisms of crack deflection and overlap when the crack collides with the wafers. The authors report a predominance of crack bridging mechanism over the particle pull-out with increasing aspect ratio of the platelets. In our studies, similar effect was observed. In the material with 3 wt.% $CaAl_{12}O_{19}$, the aspect ratio was 5:1, in the material with 6 wt.% $CaAl_{12}O_{19}$ it was 10:1.

4. Conclusions

The use of $Ca(OH)_2$ leads to the formation of the compound $CaAl_{12}O_{19}$ in the sintered alumina ceramics. The $CaAl_{12}O_{19}$ platelets are predominantly evenly distributed in the alumina matrix. As the platelet content increases, the average length of the platelets increases from 2 to 4 μm. The width of the platelets is about 0.4 μm. Increasing the $CaAl_{12}O_{19}$ content leads to decreasing the size of Al_2O_3 grains. The D50 parameter of alumina ceramics is 1.65 ± 0.02 μm. For the material containing 6 wt.% $CaAl_{12}O_{19}$, D50 is 0.95 ± 0.05 μm. The formation of $CaAl_{12}O_{19}$ platelets in the sintered Al_2O_3-ceramics leads to an increase in the fracture toughness by 48% (up to 5.2 ± 0.4 $MPa \cdot m^{1/2}$). At the same time the microhardness and density of materials decrease significantly. The increase in fracture toughness of composites containing $CaAl_{12}O_{19}$ platelets is due to the platelets fracture and crack bridging. The material containing 6 wt.% $CaAl_{12}O_{19}$ also exhibited the crack deflection mechanism for the crack propagation trajectory. Fracture toughness increases due to an increase in the aspect ratio of the platelets.

Acknowledgments. This study was fundedaccording to Russian Science Foundation research project №21-79-00306, https://rscf.ru/project/21-79-00306/21-79-00306. Research was conducted at core facility "Structure, mechanical and physical properties of materials".

References

1. M. Tian, X. D. Wang, T. Zhang. Catal. Sci. Technol. 6, 1984 (2016). Crossref
2. G. Pezzotti. Acta Metall. Mater. 41, 1825 (1993). Crossref
3. M. Machida, A. Sato, T. Kijima, H. Inoue, K. Eguchi, H. Arai. Catal. Today. 26, 239 (1995). Crossref
4. M. Machida, K. Eguchi, H. Arai. J. Am. Ceram. Soc. 71, 1142 (1988). Crossref
5. L. Liu, Y. Takasu, T. Onda, Z.-C. Chen. Ceram. Int. 46, 3738 (2020). Crossref
6. L. I. Podzorova, A. A. Il'icheva, V. P. Sirotinkin, O. S. Antonova, A. S. Baikin, V. E. Kutuzova, O. I. Pen'kova. Glas. Ceram. (English Transl. Steklo i Keramika). 78, 231 (2021). Crossref
7. V. Sirotinkin, L. Podzorova, A. Il'icheva. Mater. Chem. Phys. 277, 125496 (2022). Crossref
8. S. M. Naga, M. Elshaer, M. Awaad, A. A. Amer. Mater. Chem. Phys. 232, 23 (2019). Crossref
9. X. Huang, J. Cui, K. Guan, P. Rao. J. Aust. Ceram. Soc. 57, 1407 (2021). Crossref
10. S. M. Naga, A. M. Hassan, H. F. El-Maghraby, M. Awaad, H. Elsayed. Int. J. Refract. Met. Hard Mater. 54, 230 (2016). Crossref
11. Z. Chen, K. Chawla, M. Koopman. Mater. Sci. Eng. A. 367, 24 (2004). Crossref
12. S. Ori, T. Kojima, T. Hara, N. Uekawa, K. Kakegawa. J. Ceram. Soc. Japan. 120, 111 (2012). Crossref
13. R. Salomão, V. L. Ferreira, I. R. de Oliveira, A. D. V. Souza, W. R. Correr. J. Eur. Ceram. Soc. 36, 4225 (2016). Crossref
14. K. Vishista, F. D. Gnanam, H. Awaji. J. Am. Ceram. Soc. 88, 1175 (2005). Crossref
15. Z. D. I. Sktani, N. A. Rejab, Z. A. Ahmad. Int. J. Refract. Met. Hard Mater. 79, 60 (2019). Crossref
16. J. Sun, J. Wang, Y. Hui, X. Chen. Ceram. Int. 46, 4174 (2020). Crossref
17. Z. D. I. Sktani, N. A. Rejab, A. F. Z. Rosli, A. Arab, Z. A. Ahmad. J. Rare Earths. 39 (7), 844 (2020). Crossref
18. L. I. Podzorova, A. A. Il'icheva, O. I. Pen'kova, O. S. Antonova, A. S. Baikin, A. A. Konovalov. Inorg. Mater. 55, 628 (2019). Crossref
19. A. J. Sánchez-Herencia, R. Moreno, C. Baudín. J. Eur. Ceram. Soc. 20, 2575 (2000). Crossref
20. K. Cui, T. Fu, Y. Zhang, J. Wang, H. Mao, T. Tan. J. Eur. Ceram. Soc. 41 (15), 7935 (2021). Crossref
21. D. Asmi, I. M. Low. J. Mater. Sci. Lett. 17, 1735 (1998). Crossref
22. Z. D. I. Sktani, M. M. Ratnam, Z. A. Ahmad. J. Aust. Ceram. Soc. 52, 167 (2016).
23. U. Salma, A. Rafferty, M. Hasanuzzaman. 1–15 (2022). Crossref
24. F. Konstantiniuk, M. Tkadletz, C. Kainz, C. Czettl, N. Schalk. Surf. Coatings Technol. 410, 126959 (2021). Crossref

25. K. Niihara, R. Morena, D. P. H. Hasselman. J. Mater. Sci. Lett. 1, 13 (1982). Crossref
26. D. A. Rani, Y. Yoshizawa, K. Hirao, Y. Yamauchi. J. Am. Ceram. Soc. 87, 289 (2004). Crossref
27. M. A. Gülgün, R. Voytovych, I. Maclaren, M. Rühle, R. M. Cannon. Interface Sci. 10, 99 (2002). Crossref
28. N. Cherkasova, S. Veselov, A. Bataev, R. Kuzmin, N. Stukacheva. Mater. Chem. Phys. 259, 123938 (2021). Crossref
29. A. Altay, M. A. Gülgün. J. Am. Ceram. Soc. 86, 623 (2003). Crossref
30. A. L. N. Stevels, A. D. M. Schrama-de Pauw. J. Electrochem. Soc. 123, 691 (1976). Crossref
31. P.-L. Chen, I.-W. Chen. J. Am. Ceram. Soc. 75, 2610 (1992). Crossref
32. X. Zhang, J. Liang, J. Li, Y. Zeng, S. Hao, P. Liu, H. Na. Mater. Charact. 186, 111810 (2022). Crossref
33. S. Shi, S. Cho, T. Goto, T. Sekino. J. Alloys Compd. 835, 155427 (2020). Crossref
34. S. Shi, S. Cho, T. Goto, T. Kusunose, T. Sekino. Ceram. Int. 44, 18382 (2018). Crossref
35. S. Shi, S. Cho, T. Goto, T. Sekino. Int. J. Appl. Ceram. Technol. 18, 170 (2021). Crossref